

**Mapping the Piute Mountains, CA with Thermal Infrared Multispectral Scanner (TIMS)**

**Data**

Simon J. Hook

Jet Propulsion Laboratory, California Institute of Technology, Pasadena, CA 91109

Karl E. Karlstrom

Department of Geology, University of New Mexico, Albuquerque, NM 87131

Calvin F. Miller

Department of Geology, Vanderbilt University, Nashville, TN 37235

Kenneth J. W. McCaffrey<sup>1</sup>

Department of Earth and Planetary Sciences, Johns Hopkins University, Baltimore, MD 2218

---

<sup>1</sup> Now at the Department of Geology, Trinity College, University of Dublin, Ireland.

**Abstract**

Thermal Infrared Multispectral Scanner (TIMS) data were acquired in 1990 over the Piute Mountains, California to evaluate their usefulness for lithologic mapping in an area of metamorphosed, structurally complex, igneous and sedimentary rocks. The data were calibrated, atmospherically corrected, and emissivity variations extracted from them. There was an excellent visual correlation between the units revealed in the TIMS data and the recent mapping in the eastern side of the area. It was also possible to correct, improve and extend the recent map. For example, several areas of amphibolite were identified in the TIMS data that had been incorrectly mapped as granodioritic gneiss, and the presence of a swarm of mafic dikes, of which only a few had previously been identified, was revealed. The imagery also showed subtle color variations in the granitoid plutons, that correlated with compositional variations previously determined by extensive field and geochemical work, suggesting that TIMS are data useful for subtle compositional mapping in granitoids. In the western Piute Mountains, an area that has proven to be especially difficult to map with field and air photo methods, the TIMS data permitted the extremely heterogeneous Proterozoic schists, gneisses, and granites to be easily mapped because

the outcrop-scale compositional variability was averaged to the TIMS pixel size (12m<sup>2</sup>). In the areas of lenticular transposed gneisses, the TIMS data also accurately displayed foliation trends. TIMS data show that the Proterozoic crust in the Piute Mountains consists of granitoids (~50%), biotite gneiss (~15%), pelitic gneiss (~15%), quartzite (~10%) and amphibolite (~10%). These results indicate that TIMS data can dramatically increase the efficiency and the quality of geologic mapping in heterogenous areas where detailed mapping of lithologic contacts by traditional methods is unusually time consuming.

## **Introduction**

The majority of geologic remote sensing studies continue to focus on data from the 0.4 to 2.5µm region, which includes the visible range between 0.4 and 0.7µm, primarily due to the global availability of high spatial resolution data from the Landsat and SPOT series of satellites. These data are useful for lithological mapping, however, they are not ideal since any spectral features which permit discrimination arise from the presence of iron oxide, clay and carbonate minerals and both iron oxide and clay minerals typically arise through weathering, and only

indirectly reflect the bulk composition of the rock.

In the thermal infrared region (8-12 $\mu$ m), spectral variations typically relate to differences in the Si-O bonding of silicate minerals which usually form the bulk of the rock. Therefore, these data provide a means for discrimination based on bulk composition, which is an important criterion in some classification schemes for igneous [Streckeisen, 1976] and sedimentary rocks [Pettijohn *et al.*, 1973].

Most of the limited number of studies that have evaluated the utility of multispectral thermal infrared data for lithological mapping have been in structurally simple, unmetamorphosed areas, e.g. alluvial fans [Gillespie *et al.*, 1984], lava flows [Abrams *et al.*, 1991], hydrothermal alteration [Hook *et al.*, 1992], sedimentary basins [Lang *et al.*, 1987] and igneous rocks [Lahren *et al.*, 1988]. Far fewer studies have examined the use of these data for mapping structurally and lithologically complex areas of metamorphosed sedimentary and igneous rocks. This paper presents the results from a study undertaken to evaluate the use of thermal infrared multispectral data for lithological mapping in a structurally complex area of metasedimentary and metaigneous rocks, the Piute Mountains, California. The study area is particularly suited to this evaluation, because

this area exposes an extremely heterogeneous suite of igneous, metamorphic, volcanic and sedimentary rocks and an unusually complete tectonic record (>1.7Ga to Cenozoic) [Miller *et al.*, 1982]. The eastern side of the area was recently mapped in detail [Karlstrom *et al.*, 1993] while the western side of the area has presented difficult problems for conventional mapping and is in the process of being re-mapped.

The thermal infrared data utilized in this study were acquired with NASA's Thermal Infrared Multispectral Scanner (TIMS). TIMS is an experimental aircraft sensor and data are only available for a small number of areas, limiting the general applicability of this approach. However, a spaceborne instrument with a similar spectral coverage to TIMS is being developed and will be included on the first Earth Observing System platform (EOS-AM1). EOS-AM1 is scheduled for launch in 1998 and will provide TIMS-like data on a global basis. This spaceborne instrument is termed the Advanced Spaceborne Thermal Emission Reflectance Radiometer (ASTER) [Kahle *et al.*, 1991].

The specifications for TIMS and ASTER are presented in Tables 1 and 2. The thermal infrared data utilized in this study were acquired on July 27, 1990, under good atmospheric

conditions. Three flightlines of data were obtained over the Old Woman-Piute Mountains. The locations of these flightlines and the area described in this study are shown in Figure 1.

### **Theoretical Framework**

The reflectance and emissivity spectra of minerals exhibit diagnostic features at various wavelengths which provide a means for their remote discrimination and identification. These features are produced by electronic or vibrational processes resulting from the interaction of energy with the atoms/molecules which make up the minerals. The mineral spectra combine to produce a spectral signature for a given rock type. In order to occur, these processes require different amounts of energy and therefore are manifest in different wavelength regions. Electronic processes require the most energy and are evident in spectra covering the visible wavelength region. The fundamental vibrational processes require the least energy and evidence for them occurs beyond 2.5 $\mu\text{m}$ . In the range between 0.5 and 2.5 $\mu\text{m}$  there is an overlap of features due to electronic processes and the excitation of overtone and combination tone vibrations [Hunt, 1980].

The reflectance spectra of minerals short of 1.0 $\mu\text{m}$  are dominated by processes involving the transition metals. The most common transition metal on the surface of the earth is iron and

as a result rock spectra covering the range 0.4 to 1.0 $\mu\text{m}$  are dominated by features associated with different iron oxide-bearing minerals. Between 1.0 and 2.5 $\mu\text{m}$  mineral spectra are dominated by overtones and combinations involving the hydroxyl ion. As a result clay mineral spectra contain numerous spectral features in this wavelength range. In addition carbonate minerals display various spectral features in this wavelength range due to combination/overtone involving carbon and oxygen.

By contrast, silicate minerals, the fundamental building blocks of most rocks, exhibit numerous spectral features around 10 $\mu\text{m}$  in the thermal infrared (8-12 $\mu\text{m}$ ). Collectively, these features are referred to as the reststrahlen band. The minimum of the reststrahlen band occurs at the shortest wavelengths for framework silicates (quartz, feldspar) and at longest wavelengths for materials in which the  $\text{SiO}_4$  tetrahedra are isolated, as in orthosilicates [Hunt, 1980]. The only other feature in silicate mineral spectra between 8.5 and 12 $\mu\text{m}$  results from the H-O-Al bond and occurs near 11 $\mu\text{m}$ ; it is characteristic of aluminum bearing clay minerals [Hunt, 1980].

Other nonsilicate molecular units also give rise to spectral features in the thermal infrared including carbonates, sulphates, phosphates, oxides and hydroxides, which typically occur in

sedimentary and metamorphic rocks. Figure 2 shows the reflectance and emissivity spectra of a variety of minerals between 0.4-2.5 and 8-12 $\mu$ m.

Since rocks are composed of mixtures of minerals their spectral signature is a composite of the spectra of the individual minerals which make up the rock. This can be seen by examining the spectra of various igneous rocks in Figure 3. As the rocks become more mafic, the reststrahlen band located around 10 $\mu$ m moves to longer wavelengths. This results from the change in the dominant silicate mineral from framework silicates (e.g. quartz) to orthosilicates (e.g. pyroxene)

### **Geological Setting**

The Piute Mountains are located at the eastern edge of the Mojave Desert, east of the town of Essex on old Route 66. They are considered to be part of a relatively stable, unextended terrane between two moderately to highly extended terranes of mid-Tertiary age, the Colorado River Extensional Corridor [*Howard and John, 1987*] on the east and the Central Mojave Extensional Complex [*Dokka, 1986*] to the west. Thus this has been a key area for unraveling the pre Tertiary history of the eastern Mojave Desert [*Miller et al., 1982*]. The Piute Mountains are bounded to

the east by the NE-SW trending Little Piute fault, a normal fault along which the Little Piute Mountains have been dropped down to the southeast [Hileman *et al.*, 1990]. Immediately to the east of the Little Piute Mountains, buried by alluvium in the Ward Valley, is the inferred breakaway fault at the western margin of the Colorado River Extensional Corridor. To the west of the Piute Mountains is a little studied area which passes into the Central Mojave Extensional Complex. The Old Woman Mountains, a prominent 40-km long north trending range (Figure 1), are just south of the Piute Mountains. The Piutes-Little Piutes area includes Proterozoic supracrustal and plutonic rocks, Paleozoic through early Mesozoic metasedimentary rocks, Jurassic dikes, unmetamorphosed late Cretaceous granites and unmetamorphosed Tertiary volcanic and sedimentary strata [Howard *et al.*, 1987; Bender *et al.*, 1990; Hileman *et al.*, 1990; Miller *et al.*, 1990; Karlstrom *et al.*, 1993; Gerber *et al.*, in press]. Metamorphic and thermochronologic studies indicate that the pre-Tertiary rocks were at mid crustal levels (10-20km) in the Late Cretaceous, then ascended to the upper crust by the end of the Cretaceous [Foster *et al.*, 1989]. The area has remained in the upper crust (generally <5-6 km) since the early Tertiary [Hileman *et al.*, 1990, Foster *et al.*, 1991].

Early Proterozoic supracrustal rocks are the oldest rocks in the area (>1.7Ga). They include strongly deformed pelitic and quartzofeldspathic schists, gneisses and quartzite with minor amphibolite [*Fletcher and Karlstrom, 1990*]. These are often found interleaved with a group of granitic orthogneisses emplaced between 1710 and 1725 Ma [*Wooden et al., 1988; Wooden and Miller, 1990*]. Later in the Proterozoic, these were intruded by the Fenner Gneiss, a 1683±5 Ma K-feldspar megacrystic granite to granodiorite [*Wooden et al., 1988, Bender et al., 1990*], two-mica granites dated at 1674 Ma [*Fletcher and Karlstrom, 1990*] and the 1419±7 Ma Barrel Springs Pluton a megacrystic syenite and granite [*Gleason et al., 1988*]. This package was intruded by scattered diabase dikes believed to be between 1.1 and 1.2 Ga based on similarities with dikes dated elsewhere [*Burchfiel and Davis, 1981; Fitzgibbon, 1988*].

The Proterozoic sequence is unconformably overlain by a cratonal Palaeozoic sequence of metasedimentary rocks. The base of this sequence consists of quartzite and schist correlated with the Cambrian Wood Canyon Formation, Zabuske Formation and Bright Angel Formation which pass upward to a banded marble correlated with the lower part of the Cambrian Bonanza King Formation [*Fletcher and Karlstrom, 1990*]. The banded marble is overlain by a thick sequence of

carbonate which includes a lower massive tan-grey dolomitic marble and upper coarse grained white calcitic marble. The lower tan-grey marble is correlated with the Middle Cambrian Bonanza King Formation, the Upper Cambrian Nopah Formation and/or the Devonian Sultan formation [Stone *et al.*, 1983; Brown, 1984]. The upper white marble has been correlated with the Mississippian Redwall Limestone [Brown, 1984, Fletcher and Karlstrom, 1990].

During Mesozoic time the region underwent thrust faulting, magmatism and metamorphism [Miller *et al.*, 1982; Howard *et al.*, 1987; Foster *et al.*, 1992]. The grade of Mesozoic metamorphism ranges from greenschist facies (<450° C) in the Piute Mountains to the upper sillimanite zone of the low pressure amphibolite facies (>650° C) in the Old Womans, with pressures ranging from 2.5-4kb [Hoisch *et al.*, 1988; Foster *et al.*, 1992]. Two plutons were intruded into the Proterozoic and Palaeozoic rocks of the study area during the Late Cretaceous: the 85 Ma East Piute pluton, which was emplaced syntectonically along a thrust fault [Karlstrom *et al.*, 1993], and the Lazy Daisy Pluton, a 72 +/- Ma two-mica granite that crystallized after the peak deformation and induced the highest metamorphic grades along its margin [Hoisch *et al.*, 1988; Fletcher and Karlstrom, 1990; Foster *et al.*, 1992; Kingsbury *et al.*, in press]

The Proterozoic, Paleozoic and Mesozoic rocks are unconformably overlain by a sequence of unmetamorphosed Tertiary volcanic and sedimentary rocks. The lower part of this sequence is dominated by siliclastic sediments, basalt and basaltic andesite [Hileman *et al.*, 1990]. This is capped by the 18.5 Ma Peach Springs Tuff, which is highly variable in thickness [Hileman *et al.*, 1990; Miller and Miller, 1991]. The Peach Springs Tuff is overlain by unconsolidated Quaternary alluvium in the Piute Mountains. East-southeast trending, near vertical dikes ranging from basalt to rhyolite in composition are abundant in the eastern portion of the Piute Mountains [Hileman *et al.*, 1990].

### **Data Processing and Analysis**

The TIMS instrument measures the energy radiated from the surface in six discrete channels located between 8 and 12 $\mu$ m. Initially the TIMS data were calibrated to radiance at the sensor [Palluconi and Meeks, 1985] then atmospherically corrected to radiance at the surface using the LOWTRAN 7 radiative transfer model [Kneizys *et al.*, 1988]. LOWTRAN derives values for the atmospheric correction based on an input atmospheric profile which may be obtained from

default profiles in LOWTRAN 7, or the profile may be modified/replaced with local atmospheric data. In this study no local atmospheric data were available and the default mid-latitude winter profile was used. The default winter profile was used rather than the summer profile since the latter is far moister than would be expected for a desert area in the summer. Atmospheric correction of TIMS data is discussed in detail in *Hook et al.*, [1992].

After atmospheric correction, the ground radiance data are a function of temperature and emissivity. In this study we were interested in variations in surface emissivity since these relate to differences in composition. The emissivity information was extracted with the alpha residual technique [*Hook et al.*, 1992; *Kealy and Hook*, in press]. The resultant alpha residual spectra have a similar shape to emissivity spectra; however, the mean of each spectrum is centered on zero.

Two techniques were used to analyze the processed data. First, color composite images were produced in which processed data from TIMS channels 1, 2 and 3 were displayed in red, green and blue respectively. This color combination was selected because the majority of the rocks in the area were of felsic composition and therefore showed the greatest variation in emissivity in TIMS channels 1-4. A statistical technique which lumps the greatest variation from

all six channels into three channels such as Principal Components Analysis was not used since it is extremely difficult to relate color variations in the principal component imagery to known physical variations in emissivity. The color of an area in these images can then be related to the emissivity values of the surface in each channel. If an area has high emissivity values in channel 1 and low values in channels 2 and 3 it will appear red. If it has high values in channel 2 and low values in channels 1 and 3 it will appear green and if it has high values in channel 3 and low values in the other channels it will appear blue. If a material has high values in channels 1 and 2 and low values in channel 3 it will appear yellow since red and green combine to produce yellow. Similarly, an area with high values in channels 1 and 3 and low values in channel 2 it will appear magenta and an area with low emissivity values in channel 1 and high values in channels 2 and 3 it will appear cyan. The process of color additive mixing is described in detail in *Remote Sensing and Interpretation* by *Lillesand and Kieffer* [1979]. It should be noted that in order to create an image with good contrast, the alpha residual data from each TIMS channel used for display was scaled linearly using the mean  $\pm$  3 standard deviation for that channel. As a result the spectral shape is not preserved and it is necessary to take into account the other

materials in the scene when comparing the imagery to the spectra extracted and presented from the unscaled alpha residual data.

Second, spectra were extracted from each unit that could be discriminated in the imagery. They show the average variation in emissivity for a given area in all six TIMS channels. For example, Spectrum C - Figure 7a is from a quartzite; this is similar to the spectrum of pure quartz for the same wavelength range although of much lower spectral resolution (Figure 2). Both spectra have low emissivity values in the wavelengths covered by the first three TIMS channels and higher values in the wavelengths covered by the last three TIMS channels. This "spectral signature" indicates the surface consists of Silicon and Oxygen bonded together in a framework silicate. Unfortunately, most rocks are not mono-mineralic and as a result the spectra of multi-mineralic rocks are more complicated since they result from a mixture of the individual spectra of the minerals that make up the rock. Each spectrum presented represents the mean +/- 1 standard deviation for the group of pixels extracted from each unit. The number of pixels extracted depended on the size of the unit that could be discriminated on the imagery.

## Data Interpretation

We first discuss interpretation of the TIMS data acquired over the eastern side of the study area and contrast this with the recently completed geological map. This interpretation is then extended to the imagery acquired over the western side of the study area and used to improve the existing geologic map. The existing geologic maps for each side of the study area are shown in Figures 4 and 5. Figures 6 and 9 show TIMS color composite images for the eastern and western sides of the study area. Figures 7a, 7b and 11 show the spectra extracted from the different units and lastly, improved maps derived from the imagery are shown in Figures 8 and 12.

A variety of Precambrian rocks are shown in the color composite from the eastern side of the study area. These include deformed pelitic and mica-rich quartzofeldspathic schists and gneisses, amphibolite, quartzite, granitic orthogneiss and the Fenner Gneiss, a relatively mafic granite with abundant K-spar phenocrysts. The pelitic and mica-rich quartzofeldspathic schists and gneisses appear orange in the imagery (Figure 6 - Locality A). Examination of a mean spectrum from a group of pixels centered on locality A (Figure 7a - Spectrum A) indicates the emissivity is low in TIMS channel 3 with higher values in TIMS channels 1 and 2, hence their orange

appearance in the imagery. It should be noted that areas of mica-poor quartzofeldspathic schists do not appear orange, which suggests that this spectral signature indicates fairly aluminum-rich units. Areas of amphibolite appear white in the imagery (Figure 6 - Locality B). Examination of a mean spectrum from locality B (Figure 7a - Spectrum B) indicates the amphibolite has high emissivity values in TIMS channels 1, 2, and 3 and a minimum in channel 4. The movement of the minimum from channel 3 in the emissivity spectrum of the schists/gneisses to channel 4 in the amphibolite indicates a change from a more silicic to mafic composition as discussed earlier. The Precambrian quartzite appears very dark brown to black (Figure 6 Locality C). Examination of the mean spectrum from this area indicates the quartzite has very low emissivity values in TIMS channels 1-3, and high values in TIMS channels 4-6 (Figure 7a - Spectrum C). The spectrum does not show the well developed doublet typical of pure quartz (Figure 2). The areas of granitic orthogneiss appear red/pink (Figure 6 - Locality D). The mean spectrum from Locality D indicates the granite has a high emissivity in channel 1 and low emissivity values in channels 2 and 3 (Figure 7a -Spectrum D). By contrast, the Fenner Gneiss appears turquoise (Figure 6 - Locality E) and has similar emissivity values in channels 1 and 2 and lower values in channel 3 (Figure

7a - Spectrum E). These spectral features probably result from the Fenner granite being unusually biotite rich (>20%). This mineral is clearly not the only mineral present in the rock; however, it is typically exposed on the sky facing surfaces since any biotite rich layer provides a weak interface along which the rock readily splits. Its spectrum is not typical of a granite (see Spectrum C). The Fenner Gneiss is cut by a series of northeast-southwest trending mafic dikes which appear white on the imagery (Figure 6 - Locality F). The standard deviation of this spectrum is slightly larger than those of other units because it was difficult to find a group of homogenous pixels since the dike outcrops are fairly small.

The Precambrian sequence is overlain by a Paleozoic sequence of quartzite, carbonate and pelitic schists (Figure 4). The quartzite appears black in the color composite image (Figure 6 - locality G) and it is difficult to distinguish its spectrum from that of the older Precambrian quartzite (Figure 7a - spectra G and C), just as it was not possible to distinguish the Precambrian supracrustal amphibolite from the cross-cutting mafic dikes (Figure 7a, Spectra B and F). This indicates that any compositional variations which would manifest as emissivity differences are insufficient at the spectral resolution of TIMS to permit discrimination of the two quartzites. In

addition, in places the areal extent of the quartzite on the imagery appears far greater than the mapped area (Figures 4 and 6). This is caused by scree from the quartzite obscuring other underlying units; care should be taken in estimating the abundance of a particular unit based on the imagery alone.

The quartzite is overlain by a thin pelitic schist (Bright Angel Formation) that appears bright orange in the imagery (Figure 6 - Locality H) in spite of the very limited outcrop extent of this unit. The orange color is difficult to distinguish from the Precambrian pelitic rocks; however, the latter are a little less orange in color (Figure 7a/b - Spectra A and H) suggesting that the intensity of color may correlate with Al content. The quartzite-schist sequence is overlain by a carbonate sequence consisting of a lower banded marble, middle dolomitic marble and upper massive calcitic marble. The entire carbonate sequence appears blue on the TIMS imagery (Figure 6 - locality I). The blue appearance of the carbonate results from its having high emissivity values in TIMS channel 3 compared to other materials in the scene (Figure 7b - Spectrum I). The diagnostic feature of calcite is a small sharp feature centered on  $11.2\mu\text{m}$  associated with C-O bonding (Figure 2). This feature moves to slightly longer wavelengths as the composition changes

from calcite to dolomite.

During Mesozoic time the Precambrian and Palaeozoic sequence was metamorphosed and then intruded in the Late Cretaceous by two granitoids, the East Piute Pluton and the Lazy Daisy Pluton (Figure 6 - Localities J and K). The spectra from these areas are very similar to the Precambrian granite spectrum from locality D (Figures 7a and 7b - Spectra D, J and K). Parts of the western margin of the East Piute Pluton are extremely felsic due to fractionation [Karlstrom *et al.*, 1993] and these appear much redder on the imagery (Locality O in Figure 23). This subtle difference was defined by geochemical studies and is important in documenting the emplacement history of the pluton. This difference suggests that TIMS could be used for very subtle compositional mapping of granites. In fact, it appears that the following colors correspond to a trend from more mafic to felsic plutons: White - Amphibolite (Locality F), Blue - Fenner Granodiorite with biotite and hornblende (Locality E), Red/orange - Precambrian two-mica granite (Locality P), Pink - Cretaceous two-mica granite (Locality K), Red - leucocratic granite (Locality O).

The Precambrian, Paleozoic and Mesozoic rocks are unconformably overlain by Tertiary

volcanic and sedimentary rocks. The lower part of the sequence is dominated by basalt -and basaltic-andesite -rich conglomerates and basaltic andesite, both of which appear grey/white on the imagery (Figure 6 - locality L). The spectrum from this lithology is similar to the amphibolite spectra (Figures 7a and 7b - Spectra B, F and L); consistent with their similar compositions. The basalt-rich conglomerates are overlain by the Peach Springs tuff, which has a maroon/plum color in the imagery (Figure 6 localities M and N, Figure 7b spectra M and N). The maroon-colored areas correspond to the base of the Peach Springs Tuff while the upper part of the unit appears plum colored. Generally, the tuff becomes more altered and devitrified upwards and the clear difference in color suggests that TIMS data may be useful in deciphering subtle internal variations within single ash-flow units. At the very top of the unit there is a grey unit in some parts of the imagery which is fairly difficult to distinguish. It was not possible to identify this unit in the field and the cause for this color difference remains undetermined.

Comparison of the geological map at the eastern side of the study area taken from [Karlstrom *et al.*, 1993] with the image indicates that, based on composition, the TIMS imagery permits excellent discrimination of the mapped geological units (Figures 4 and 6). However, if two

units have a similar bulk composition but differ in texture or the presence of a minor constituent it may not be possible to separate them on the imagery, for example the Precambrian and Mesozoic granites or Precambrian and Paleozoic quartzites. Although there is good general agreement between the geological map and the imagery, there are some areas where the imagery led quickly to improvements of the map. For example, the area southeast of the East Piute pluton was mapped from traditional 1:24,000 air photos, which show variations in brightness primarily due to iron oxide differences that result from weathering and only indirectly relate to composition, as opposed to the TIMS data that show variations in silicate mineralogy which often relates directly to differences in bulk composition. The TIMS data show two large areas of what appears to be amphibolite (Figure 6 - locality B), which had been mapped as Fenner Gneiss (Figure 4). These units weather to a similar color to the Fenner Gneiss and were mapped from an air photo, hence their confusion on the air photos but not in the TIMS data. It is also far easier to distinguish the dike swarm on the imagery (Locality F, Figure 6). The weathering process in this area results in each unit being coated with desert varnish. The varnish makes it difficult to distinguish units in the air photos, therefore necessitating close inspection in the field. This is less

of a problem in the thermal infrared since desert varnish is partially transparent at these wavelengths and the surface response is dominated by the underlying silicate composition rather than the composition of the varnish. Figure 8 shows the compositional map of the east part of the study area derived from the TIMS data.

The combined detailed field mapping and TIMS compositional map of the eastern area provide information to produce a similar map in the less well mapped western areas. This area is currently being mapped in detail, providing an opportunity to check the accuracy of a compositional map derived from TIMS in a relatively unknown area. Figure 9 is a color composite image of the western side of the study area. There is some overlap between this image and the image from the eastern side of the area (Figure 6). Figure 10 shows an air photo acquired over the study area simultaneously with the TIMS data. While some of the mapped units can be distinguished due to differences in brightness in the air photo, many more units can be discriminated in the TIMS image. For example, the quartzites, which appear black in the TIMS image and run N-S, are difficult to distinguish in the air photo.

Several units in addition to those identified on the eastern side of the study area are

apparent in the imagery. In the southwest part of the image is a large pink colored area associated with the Barrel Spring Pluton (Figure 9 - locality A). The Barrel Spring Pluton has been subdivided into areas of quartz syenite, mafic syenite, K-spar porphyry and porphyry dikes. It is not possible to distinguish the porphyry dikes from the quartz syenite but it is just possible to separate the K-spar porphyry from the quartz syenite, (the former has a brown tint), further illustrating that TIMS is able to map subtle compositional differences in granitoids within a single pluton. Figure 11 shows spectra from these two areas, spectra A (porphyry) and B (syenite). A mafic and felsic injection zone has been mapped in one of the northern areas of quartz syenite. In the imagery this zone appears to swing further to the south (?). It was not possible in the field to establish the difference between the southern part of this zone and the main quartz syenite. Further south there is a dark blue unit which has been mapped as Precambrian metasedimentary rocks (Figure 9 - locality C). To the east of the northern parts of the Barrel Springs pluton is a unit that is striped yellow and turquoise/blue in appearance. This unit becomes more turquoise/blue further east. It was originally mapped as granite augen gneiss, but the TIMS data suggest the yellow areas are garnet staurolite gneiss (pelitic and muscovite rich) [Figure 11 - Spectra Da and

Db] whereas the turquoise/blue areas are quartz and biotite rich (Figure 11 - Spectrum E). This has been substantiated by field mapping. Broad bands dominated by pelitic (orange) versus biotite-rich (turquoise) gneisses are readily defined at a 1:24,000 scale of the imagery but are difficult to map in the field due to the smaller scale interfingering of the various units. Thus TIMS helps define the foliation traces as well as compositional differences. Several areas were strongly mylonitized and compositionally were quartz and biotite rich. The quartz + biotite rich areas may have originated from both sedimentary and granitic rocks. The color of the quartz + biotite rich unit is similar to the Fenner Gneiss, which is also biotite rich. However, while these units have a similar emissivity in TIMS channels 1, 2 and 3, they have very different emissivity values at longer wavelengths (Figure 7a - Spectrum E and Figure 11 Spectrum E). Further east this unit passes into a black and orange unit, that comprises the Precambrian quartzite and pelites/quartzofeldspathic schists and gneiss. The major bands of quartzite which form part of the interlayered sequence of quartz and pelite are very distinct and had not been recognized in this area previously. This unit then passes into a red/plum unit interpreted to be the Precambrian granitic orthogneisses. In places the plum unit is clearly a river terrace, but compositionally the

surface of the terrace is not dissimilar to that of a granite (labelled T, Figure 9). The terrace can easily be recognized on the air photo. The fact that units with a similar bulk composition appear identical in the imagery was particularly advantageous for grouping together heterogeneous units. For example, in the field it can be extremely difficult to map the Precambrian quartzofeldspathic schists and gneisses since they exhibit large textural differences and large variations in composition on a local scale. By contrast since each pixel in the image represents the emissivity from 12m<sup>2</sup> square any local compositional/textural variations are averaged and in some cases it is far easier to recognize bulk compositional boundaries.

A compositional map was derived from the TIMS data (Figure 12). This is clearly far more detailed than the existing geologic map for the area (Figure 5). This map was partially field-checked and showed excellent agreement with the actual geology. It is being incorporated into the latest geologic map under preparation for the western side of the study area and has proven particularly useful for mapping the Precambrian sediments, the extent of which were only very roughly known until this study. The TIMS data suggest that the Proterozoic crust in the Piute Mountains contains roughly equal proportions of granitoids and supracrustal gneisses. Further, the

supracrustal gneisses contain roughly equal proportions of pelitic and biotite-rich gneisses (~30%) with subordinate but still voluminous, clean quartzites (~15%) and amphibolites (~15%). The supracrustal package in the eastern area, in the hanging wall of the Fenner shear zone, is more amphibole rich, whereas the western area (footwall) is more pelitic rich. Thus the TIMS data are useful for quick estimates of the composition of the Proterozoic crust and may help distinguish tectonic blocks composed of different Proterozoic packages.

### **Summary and Conclusions**

In July of 1990 Thermal Infrared Multispectral Scanner (TIMS) data were acquired over the Old Woman and Piute Mountains, California. These data were obtained, in part, to evaluate their use for lithological mapping in a structurally complex area of metamorphosed sedimentary and igneous rocks. The Piute Mountains were particularly well suited to this study because of their extreme lithologic heterogeneity and because the eastern side of the mountains were recently mapped in moderate detail [Karlstrom *et al.*, 1993] and the western side of the mountains are currently being re-mapped.

Initially the TIMS data were calibrated and atmospherically corrected. The resultant ground radiance data contain information relating to the temperature and emissivity of the surface. Variations in surface emissivity indicate differences in composition and provide a means for remote lithological mapping. The emissivity information was extracted from the ground radiance data by using the alpha residual technique. A color composite image was then created for the eastern and western side of the Piutes by displaying the alpha residual data from the first three TIMS channels in red, green and blue, respectively.

It was possible to discriminate the majority of lithological units recently mapped on the eastern side of the study area with the color composite image. Emissivity differences in the image were related to variations in the silicate composition of the lithological units. However, certain units that were mapped on the ground by the presence of a minor constituent or some other geologic property, e.g. relative age or deformation intensity, could not be mapped in the TIMS data. This demonstrates that differences in silicate composition can be reliably mapped by TIMS regardless of fabric. Other additional units were identified which had been incorrectly mapped.

The compositional map derived from the eastern side of the study area was then used to assist in producing a compositional map from the TIMS data for the western side of the area. This map agreed with the existing geologic map and in addition permitted the discrimination of many more previously unmapped geologic units. The TIMS data were especially useful for mapping the metamorphosed Precambrian metasedimentary rocks which are particularly heterogenous and difficult to distinguish on the field scale but appear as coherent, readily mappable packages in the TIMS data. This is due to the TIMS data providing an average composition for each 12m<sup>2</sup> pixel. For example, the imagery indicated the presence of large areas of Precambrian quartzite and pelitic gneiss in the western Piute Mountains and a few small areas in the eastern Piutes that had not been recognized until this study. Thus, Proterozoic sedimentary sequences in this area of the Mojave were perhaps more compositionally evolved (richer in quartz and aluminum) than many of the volcanic-rich Proterozoic supracrustal packages in central Arizona. The compositional map is being used in conjunction with standard field mapping techniques to produce a new geologic map and revise the geologic history for the western Piute Mountains.

In conclusion, TIMS data are a very valuable tool for assisting in the mapping of

structurally complex areas of metasedimentary and metaigneous rocks. They permit variations in the silicate composition of the surface to be discriminated and in most cases identified. As these images become more readily available, they should become a standard tool for mapping in complex, well-exposed terrains.

### **Acknowledgements**

The research described in this paper was carried out in part at the Jet Propulsion Laboratory, California Institute of Technology, under a contract with the National Aeronautics and Space Administration.

Research support for Karlstrom and Miller was provided by National Science Foundation grants EAR8904675 and EAR 8904320 respectively.

Reference herein to any specific commercial product, process, or service by trade names, trademark, manufacturer or otherwise does not imply endorsement by the United States or the Jet Propulsion Laboratory, California Institute of Technology.

## References

Abrams, M. J., E. A. Abbott, and A. B. Kahle, Combined Use of Visible, Reflected Infrared and Thermal Infrared Images for Mapping Hawaiian Lava Flows. *J. Geophys. Res.*, 96, 475-484, 1991.

Bender, E. E., C. F. Miller, and J. L. Wooden, The Fenner Gneiss and associated units: An Early Proterozoic composite batholith, Piute and Old Woman Mountains, CA. *Geol. Soc. Am. Abstr. Programs*, 22, 7, 1990.

Brown, H., Discussion: Correlation of metamorphosed Palaeozoic strata of the southeastern Mojave Desert Region, California and Arizona. *Geol. Soc. Am. Bull.* 95, p. 1482-1485, 1984.

Burchfiel, B. C., and G. A. Davis, Mojave and environs, in *The Geotectonic Development of California, Rubey Volume 1*, edited by W. G. Ernst, pp. 217-252, Prentice-Hall,

Englewood Cliffs, N. J., 1981.

Dokka, R. K., Patterns and modes of early Miocene crustal extension, Central Mojave Desert, California, Extensional Tectonics of the South-western United States, edited by Mayer, L., Spec. Pap. *Geol. Soc. Am.* 208, 75-96, 1986.

Fitzgibbon, T. T., Tectonic significance and characteristics of middle Proterozoic diabase sheets in southeastern California and Arizona, (*abstract*); *Geol. Soc. Am. Abstr. Programs*, 20, 160, 1988.

Fletcher, J. M., and K. E. Karlstrom, Late Cretaceous ductile deformation, metamorphism and plutonism in the Piute Mountains, eastern Mojave Desert, *J. Geophys. Res.*, 95, 487-500, 1990.

Foster, D. A., T. M. Harrison, and C. F. Miller, Age, inheritance and uplift history of the

Old Woman-Piute Batholith, California and implications for K-feldspar age spectra, *J. Geol.*, *97*, 232-243, 1989.

Foster, D. A., D. S. Miller, and C. F. Miller, Tertiary Extension in the Old Woman Mountains Area, California: Evidence from apatite fission-track analysis. *Tectonics*, *10*, 875-886, 1991.

Foster, D. A., C. F. Miller, T. M., Harrison, and T. D. Hoisch, Timing and character of metamorphism and tectonism in the Old Woman Mountains area, California: evidence from  $^{40}\text{Ar}/^{34}\text{Ar}$  thermochronology and thermobarometry, *Geol. Soc. Am. Bull.*, *104*, 176-191, 1992.

Gerber, M. E., C. F., Miller, and J. L. Wooden, Plutonism at the interior of the Jurassic Magmatic Belt, Mojave Desert CA, Jurassic Magmatism and Tectonism in the Cordillera, edited by Miller, D. M. and R. M. Tosdal, *Spec. Pap. Geol. Soc. Am.*, (in press).

Gillespie, A. R., A. B. Kahle, and F. D. Palluconi, Mapping Alluvial Fans in Death Valley,

California using Multichannel Thermal Infrared Images, *Geophys. Res. Letters*, 11, 1153-

1156, 1984.

Gleason, J. D., C. F. Miller, and J. L. Wooden, Barrel Spring alkalic complex: 1.4 Ga

anorogenic plutonism in the Old Woman-Piute Range, eastern Mojave Desert, California

(abstract), *Geol. Soc. Am. Abstr. Programs*, 20, 164, 1988.

Grove, C. I., S. J. Hook, and E. D. Paylor II, Laboratory Reflectance Spectra of 160 Minerals,

0.4-2.5 Micrometers. *JPL Publ.*, <sup>92-2</sup>95-2, 1992.

Hileman, G. E., C. F. Miller, and M. A. Knoll, Mid-Tertiary structural evolution of the Old

Womans Mountain Area: Implications for crustal extension across southeastern California,

*J. Geophys. Res.*, 95, 581-597, 1990.

Hoisch, T. D., C. F. Miller, M. T. Hiezler, T. M. Harrison, and E. F. Stoddard, Late Cretaceous regional metamorphism in southeastern California, in *Metamorphism and Crustal Evolution of the Western United States, Rubey Volume VII*, edited by W. G. Ernst, pp. 538-571, Prentice-Hall, Englewood Cliffs, N. J., 1988.

Hook, S. J., A. R. Gabell, A. A. Green, and P. S. Kealy, A Comparison of Techniques for Extracting Emissivity Information from Thermal Infrared Data for Geologic Studies, *Remote Sens. Environ.*, 42, 123-135, 1992.

Howard, K. A., and B. E. John, Crustal extension along a rooted system of imbricate low-angle faults, Colorado River Extensional Corridor, California and Arizona, edited by M. P. Coward, J. F. Dewey, and P. L. Hancock, *Spec. Publ. Geol. Soc. London*, 28, 299-311, 1987.

Howard, K. A., B. E. John, and C. F. Miller, Metamorphic Core Complexes, Mesozoic

ductile thrusts, and Cenozoic detachments: Old Woman Mountains -Chemehuevi Mountains transect, California and Arizona. edited by G. J. Davis and E. M. Vanderwolder, *Spec. Pap. Ariz. Bur. Geol. Min. Technol.*, 5, 365-382, 1987.

Hunt, G. R., Electromagnetic Radiation: The communication link in remote sensing, in *Remote Sensing in Geology*, pp. 5-45, edited by B. S. Siegal and A. R. Gillespie, pp. 5-45, John Wiley and Sons, New York, 1980.

Kahle, A. B., F. D. Palluconi, S. J. Hook, V. J. Realmuto, and G. Bothwell, The Advanced Spaceborne Thermal Emission and Reflectance Radiometer (ASTER), *Internat. J. Imaging Systems Technol.*, 3, 144-156, 1991.

Karlstrom, K. E., C. F. Miller, J. A. Kingsbury, and J. L. Wooden, Pluton emplacement along an active ductile thrust zone, Piute Mountains, southeastern California: Interaction between deformational and solidification processes. *Geol. Soc. Am. Bull.*, 105, 213-230,

1993.

Kealy, P. S., and S. J. Hook, Separating temperature and emissivity in thermal infrared multispectral scanner data: Implications for recovering land surface temperatures, *Geosci. Remote Sens.*, (in press).

Kingsbury, J. A., C. F. Miller, J. L. Wooden, and T. M. Harrison, Monazite paragenesis and Uranium-Lead systematics in rocks of the Eastern Mojave desert, California: Implications for thermochronometry, *Chemical Geology*, (in press).

Kneizys, F. X., E. P. Shettle, L. W. Abreu, J. H. Chetwynd Jr., G. P. Andersen, W. O. Gallery, J. E. A. Selby, and S. A. Clough, Users guide to LOWTRAN 7, Environmental Research Paper 1010, *Tech. Rep. AFGL-TR-88-0177*, Air Force Geophys. Lab., Bedford, Mass., 1988.

Lahren, M. M., R. A. Schweickert, and J. V. Taranik, Analysis of the northern Sierra accreted terrain, California, with airborne thermal infrared multispectral scanner data, *Geology*, 16, 525-528 1988.

Lang, H. R., S. L. Adams, J. E. Conel, B. A. McGuffie, E. D. Paylor, and R. E. Walker, Multispectral remote sensing as stratigraphic and structural tool, Wind River Basin and Big Horn Basin Areas, Wyoming, *Am. Assoc. Petrol. Geol. Bull.*, 71, 389-403, 1987

Lillesand, T. M., and R. W. Kieffer, *Remote Sensing and Image Interpretation*, John Wiley and Sons, New York, 1979.

Lyon, R. J. P., Analysis of rocks by spectral infrared emission (8 to 25 microns), *Econ. Geol.*, 60, 715-736, 1965.

Miller, C. F., K. A. Howard, and T. D. Hoisch, Mesozoic thrusting, metamorphism, and

plutonism, Old-Woman-Piute Range, southeastern California, in *Mesozoic-Cenozoic tectonic evolution of the Colorado River, region, California-Arizona-Nevada*, edited by E. G. Frost, and D. L. Martin, pp. 561-581, Cordilleran Publishers, San Diego, California, 1982.

Miller, C. F., J. L. Wooden, V. C. Bennett, J. E. Wright, G. C. Solomon, and R. W. Hurst, Petrogenesis of the composite peraluminous-metaluminous Old Woman-Piute Range batholith, southeastern California; isotopic constraints., in *The nature and origin of Cordilleran magmatism* edited by J. L. Anderson, Geol. Soc. Am. Mem., 174, 99-109, 1990.

Miller, J. S., and C. F. Miller, Tertiary Extension-Related Volcanism, Old Woman Mountains Area Eastern Mojave Desert, California, *J. Geophys. Res.*, 96, 629-643. 1991.

Palluconi, F. D., and G. R. Meeks, Thermal infrared multispectral scanner (TIMS): An

investigator's guide to TIMS data, *JPL Publ.*, 85-32, 1985.

Pettijohn, F.J., P. E. Potter, and R. Siever, *Sand and Sandstone*, Springer Verlag, New York, 1973.

Salisbury, J. W., L. S. Walter, N. Vergo, and D. M. D'Aria, *Mid-Infrared (2.1-25 $\mu$ m Spectra of Minerals*, Johns Hopkins University Press, Baltimore, 1992.

Stone, P., K. A. Howard, and W. Hamilton, Correlation of Palaeozoic strata of the southeastern Mojave Desert region, California and Arizona: *Geol Soc. Am. Bull.* 94, 1135-1147, 1983.

Streckeisen, A., To each plutonic rock its proper name, *Earth Science Review*, 12, 1-33, 1976.

Vickers, R. S., and R. J. P. Lyon, Infrared sensing from spacecraft - a geological interpretation. *American Institute of Aeronautics and Astronautics Thermophysics Specialist Conference*,

Paper No 67-284, New Orleans, Louisiana April 17-20, 1967.

Wooden, J. L., D. M. Miller, and K. A. Howard, Early Proterozoic chronology of the eastern Mojave Desert (abstract), *Geol. Soc. Am. Abstr. Programs*, 20, 243, 1988.

Wooden, J. L., and D. M. Miller, Chronologic and isotopic framework for Early Proterozoic crustal evolution in the Eastern Mojave desert regions, S.E. California, *J. Geophys. Res.*, 95, 133-146, 1990.

## Figures

Figure 1. Location of the study area. Centerline of TIMS flights also shown. Box indicates area evaluated in this study.

Figure 2. Reflectance (left) and emissivity spectra (right) of a variety of rocks and minerals in the wavelength regions 0.4-2.5 microns and 8-12 microns. Reflectance spectra from *Grove et. al.*, [1992]. Emissivity spectra from *Salisbury et. al.*, [1992]. Hashed area in reflectance data indicates the position of the atmospheric absorption bands which absorb any reflected energy from the surface.

Figure 3. Emissivity spectra of igneous rocks. Note the shift to longer wavelengths of the main absorption band as the rock becomes more mafic. Redrawn from *Lyon*, [1965] and *Vickers and Lyon*, [1967].

Figure 4. Geology of the eastern side of the study area based on *Karlstrom et. al.*, [1993].

Figure 5. Geology of the western side of the study area based on an unpublished compilation of maps from Karlstrom, COWPIE compiler.

Figure 6. TIMS color composite image for the <sup>eastern</sup> western side of the study area created by displaying the alpha residual data from channels 1, 2 and 3 in red, green and blue respectively. Labels A through N indicate regions used to extract average pixel spectra shown in Figure 7. Labels O and P identify additional areas described in text.

Figure 7a. Average TIMS spectra extracted from areas labelled A through H on Figure 6. Each three line set indicates the mean  $\pm$  1 standard deviation. A - Precambrian pelitic and aluminous psammitic metasediments (schists and paragneisses), B - Precambrian amphibolite, C - Precambrian quartzite, D - Precambrian orthogneiss, E - Precambrian biotite granite, F - Precambrian NE-SW amphibolite dikes, G - Palaeozoic quartzite, H - Palaeozoic pelitic schist.

Figure 7b. Average TIMS spectra extracted from areas labelled I through N on Figure 6. Each

three line set indicates the mean  $\pm$  1 standard deviation. I - Palaeozoic carbonate, J - Cretaceous granodiorite (E. Piute pluton), K - Cretaceous two mica granite (Lazy Daisy pluton), L - Tertiary basalt rich conglomerate, M - Tertiary tuff (lower), N- Tertiary tuff (upper).

Figure 8. Compositional map of the eastern side of the study area interpreted from the TIMS alpha residual image (Figure 6) and the TIMS alpha residual spectra (Figures 7a and 7b).

Figure 9. TIMS color composite image for the <sup>western</sup> eastern side of the study area created by displaying the alpha residual data from channels 1, 2 and 3 in red, green and blue respectively. Labels A through E indicate regions used to extract average pixel spectra shown in Figure 11. Label T indicates a river terrace.

Figure 10. Air Photo covering the southwest part of the study area taken simultaneously with the acquisition of the TIMS data.

Figure 11. Average TIMS spectra extracted from areas labelled A through E on Figure 9. Each three line set indicates the mean  $\pm$  1 standard deviation. A - Precambrian quartz syenite (Barrel Springs), B - Precambrian K-spar deformed syenite (Barrel Springs), C - Precambrian sediments, Da - Precambrian quartz augen gneiss, Db - Precambrian quartz augen gneiss, E - Precambrian quartz augen gneiss.

Figure 12. Compositional map of the western side of the study area interpreted from the TIMS alpha residual image (Figure 9) and the TIMS alpha residual spectra (Figure 11). Some features shown here as rock are alluvium filled washes as discussed in the text.

## Tables

Table 1. Summary specifications for the Thermal Infrared Multispectral Scanner (TIMS). (It should be noted that the channel positions shown for TIMS change slightly from time to time, and one must use the values appropriate for any given flight (Palluconi and Meeks, 1985). The center positions of each of the channels used in this study were 8.407, 8.801, 9.204, 9.933, 10.703, 11.625 $\mu\text{m}$ ).

Table 2. Summary specifications for the Advanced Spaceborne Thermal Emission Reflectance Radiometer (ASTER).

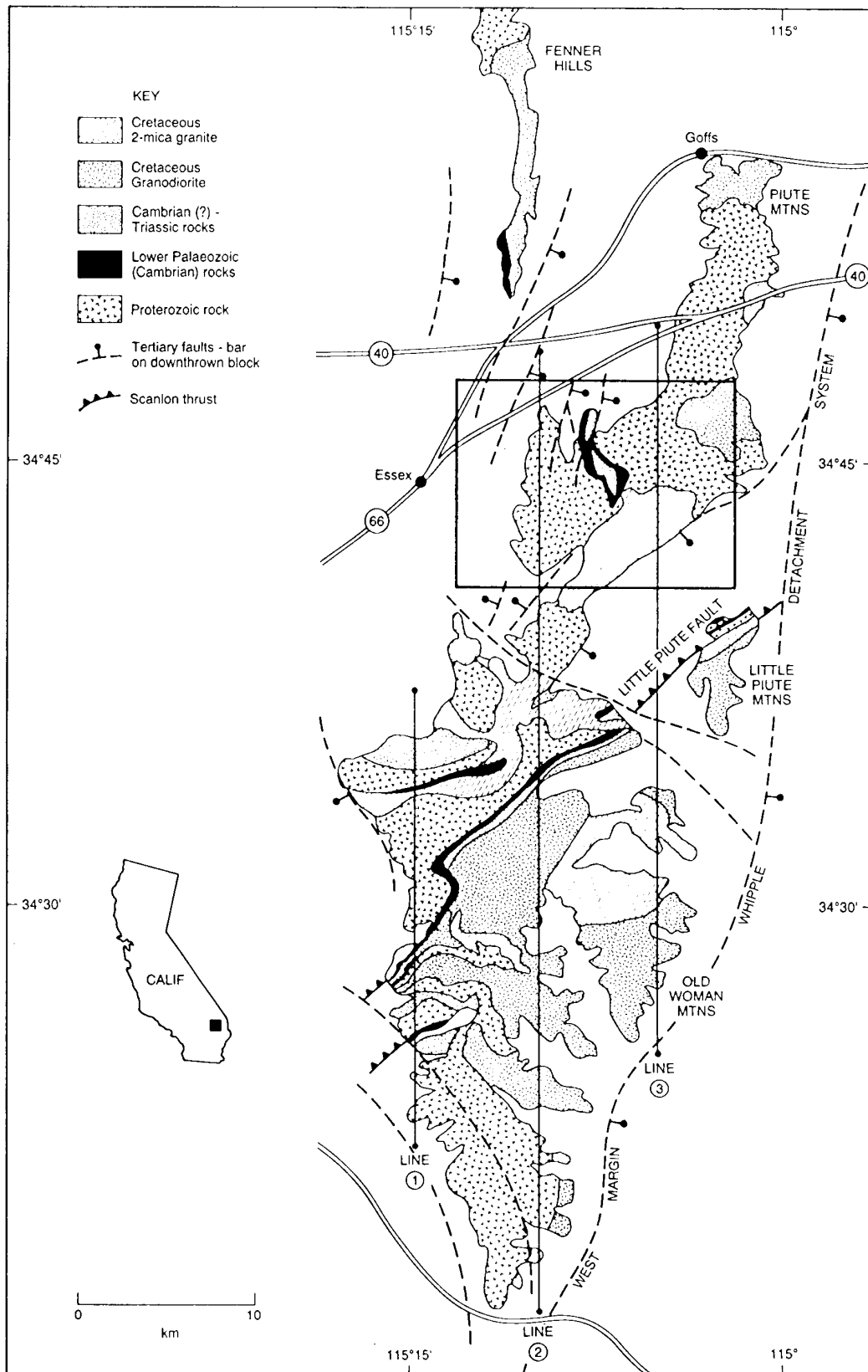


Figure 1.

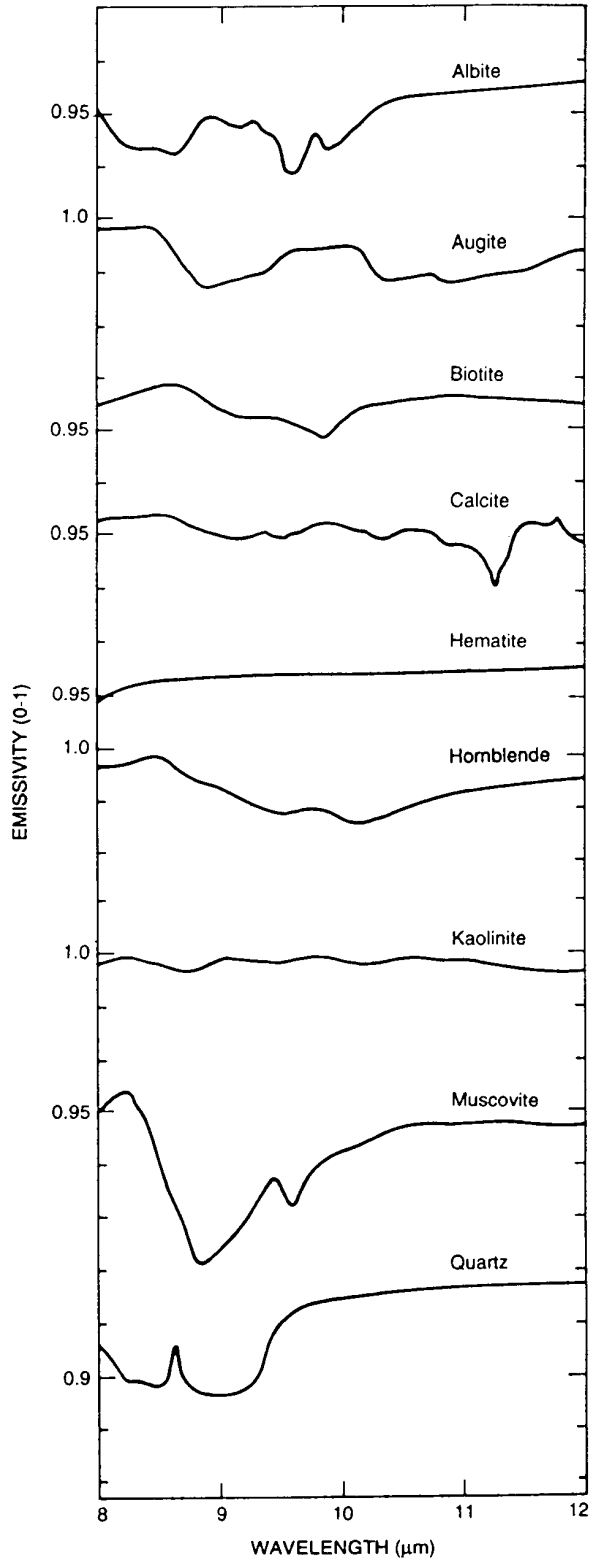
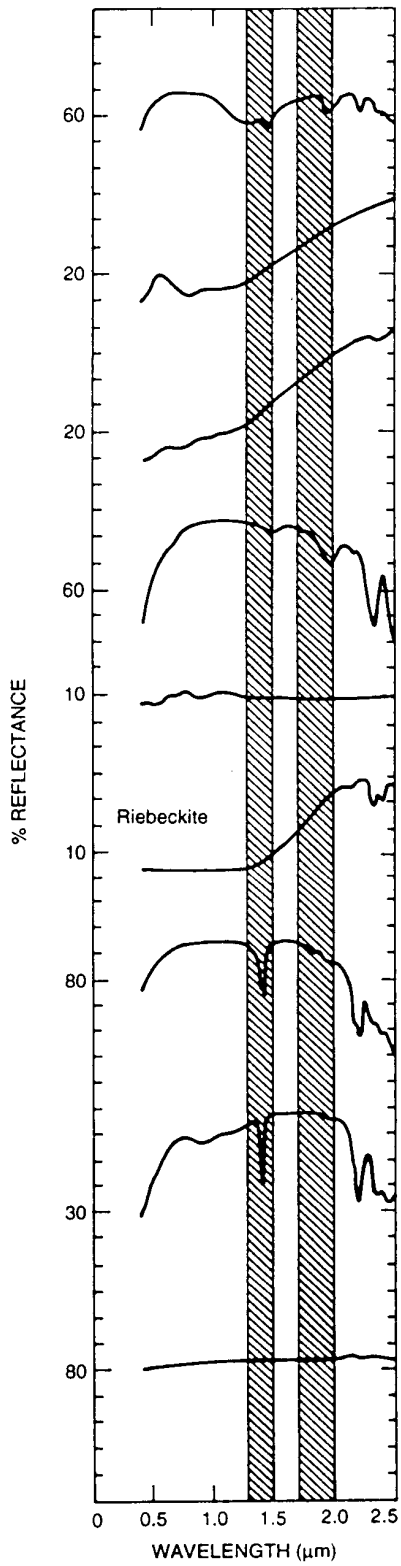


Figure 2

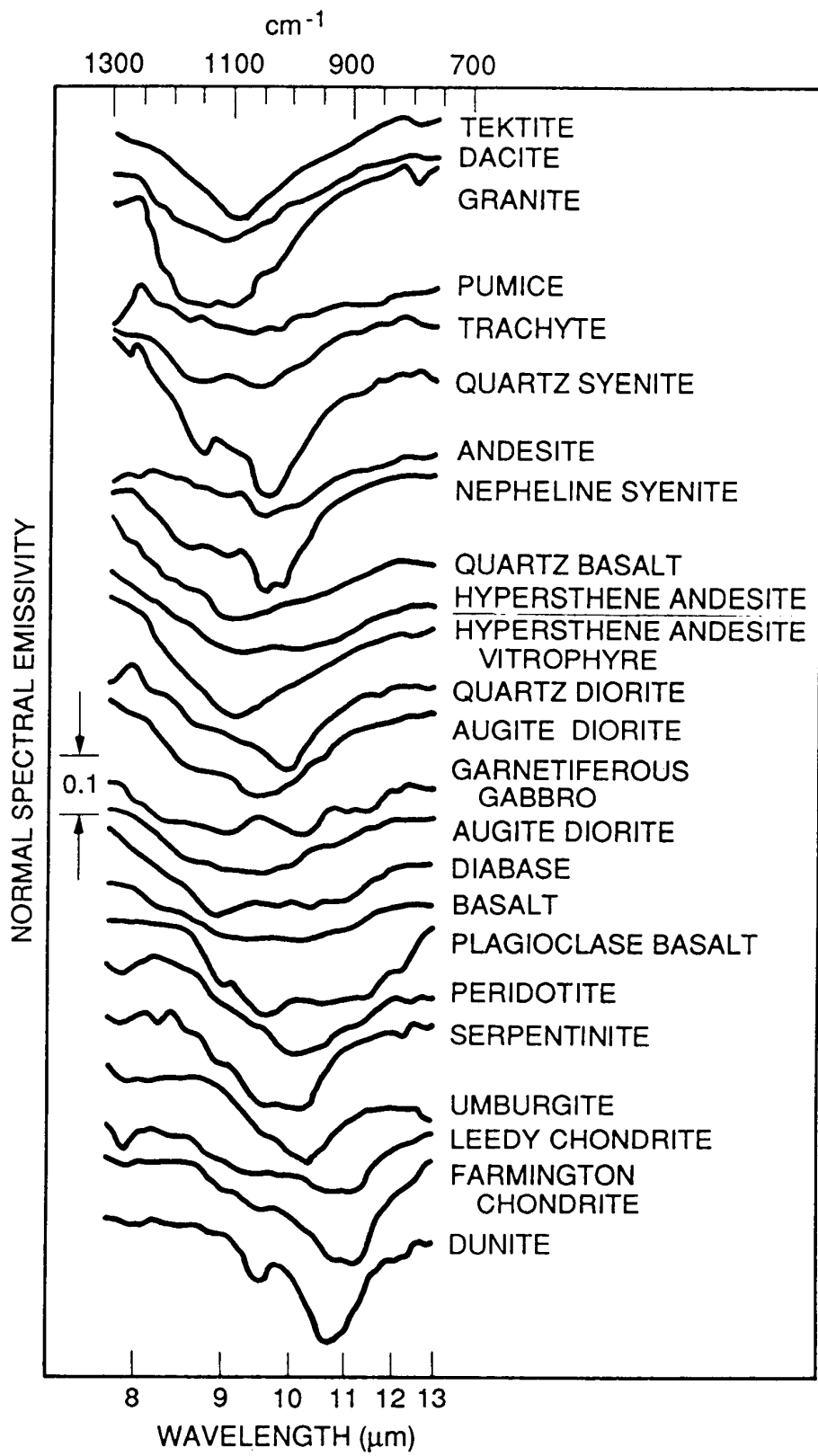


Figure 3

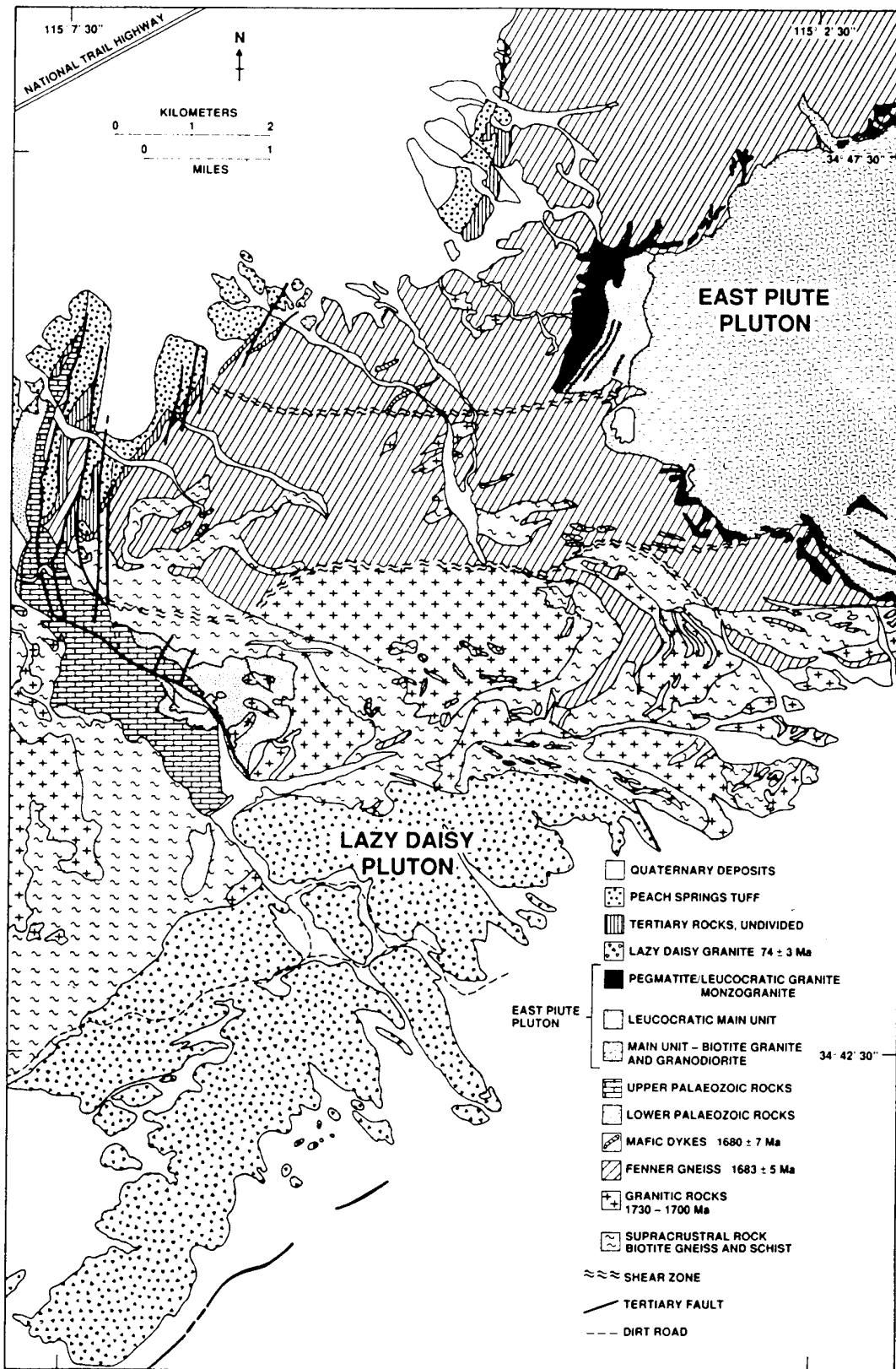


Figure 41

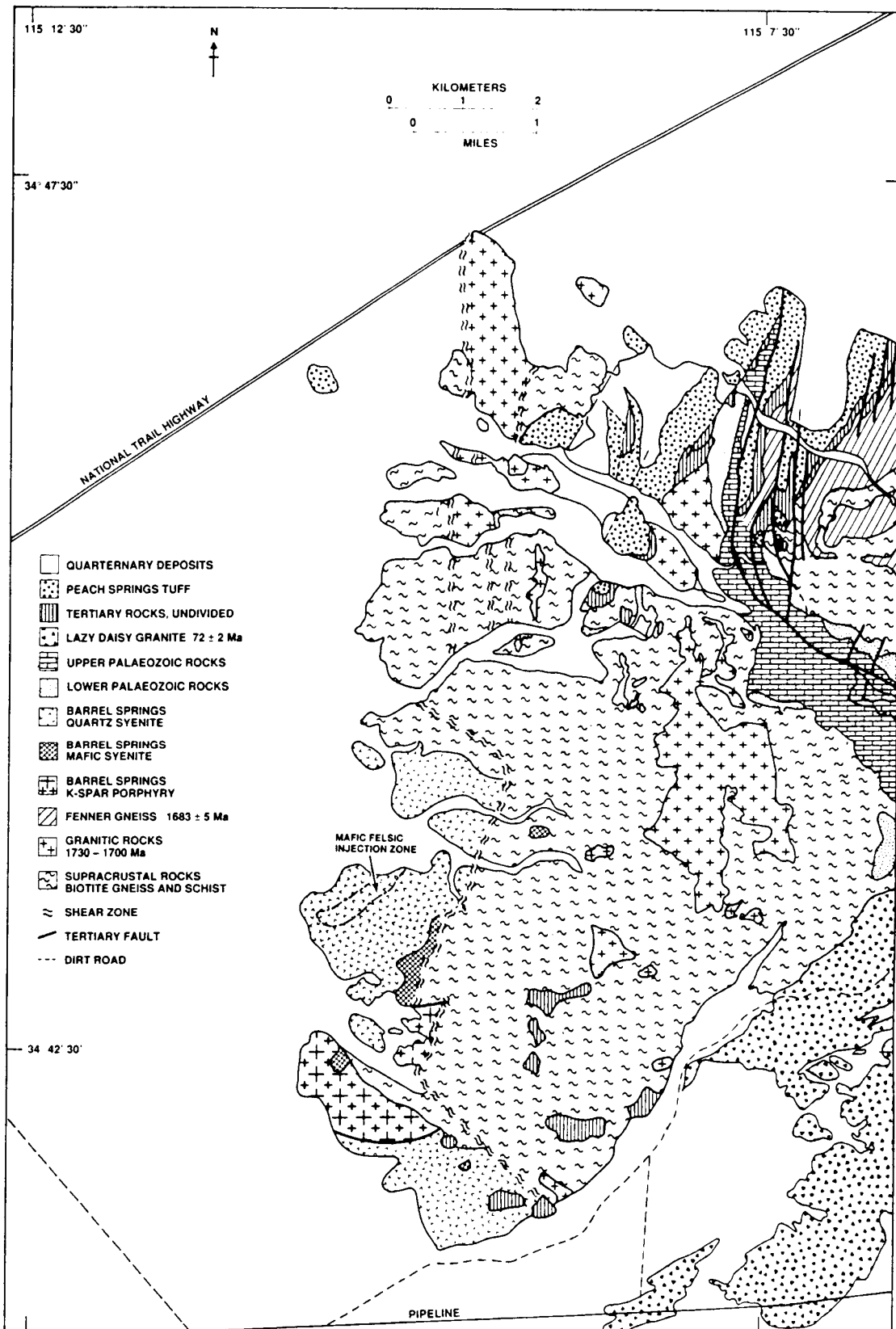


Figure 5



1950-51

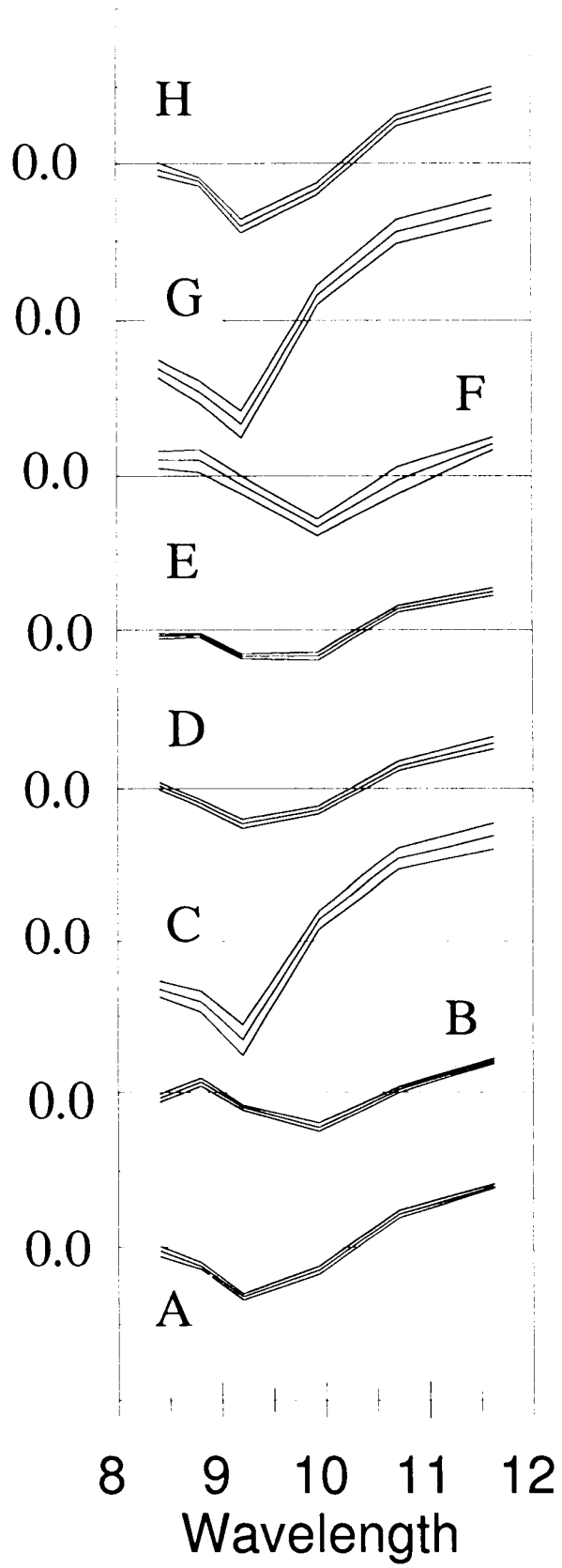


Figure 7a

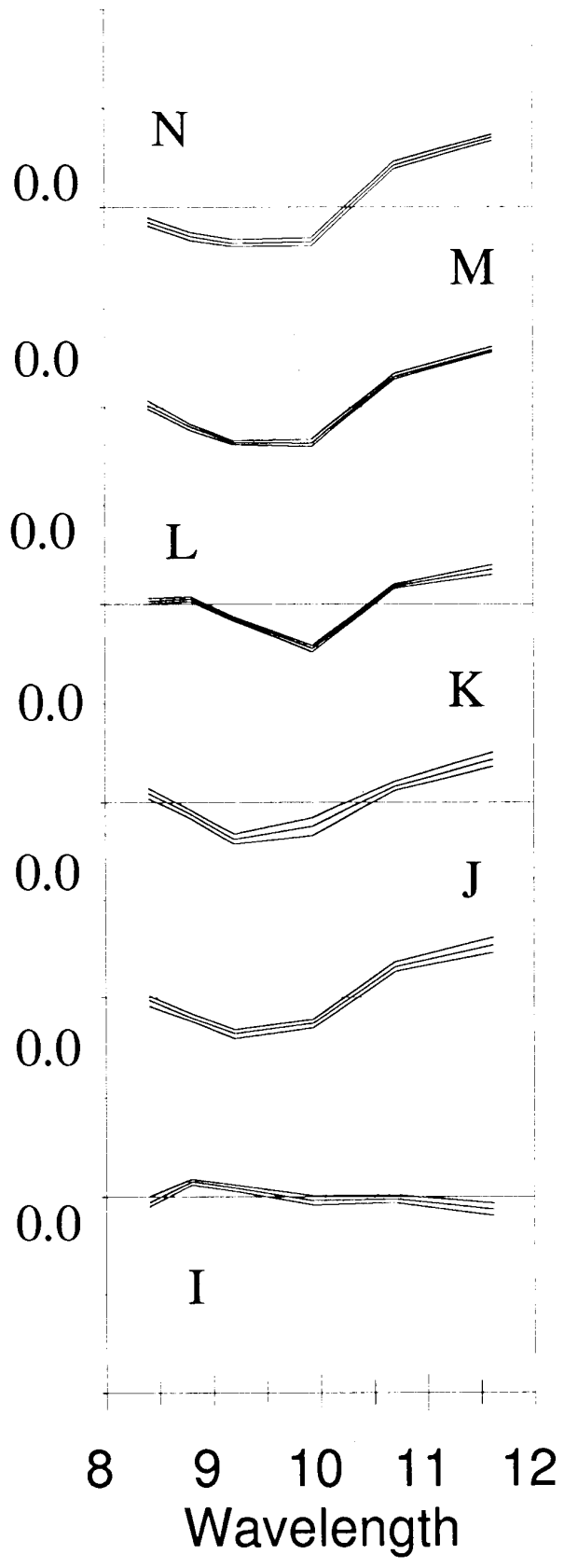


Figure 7b

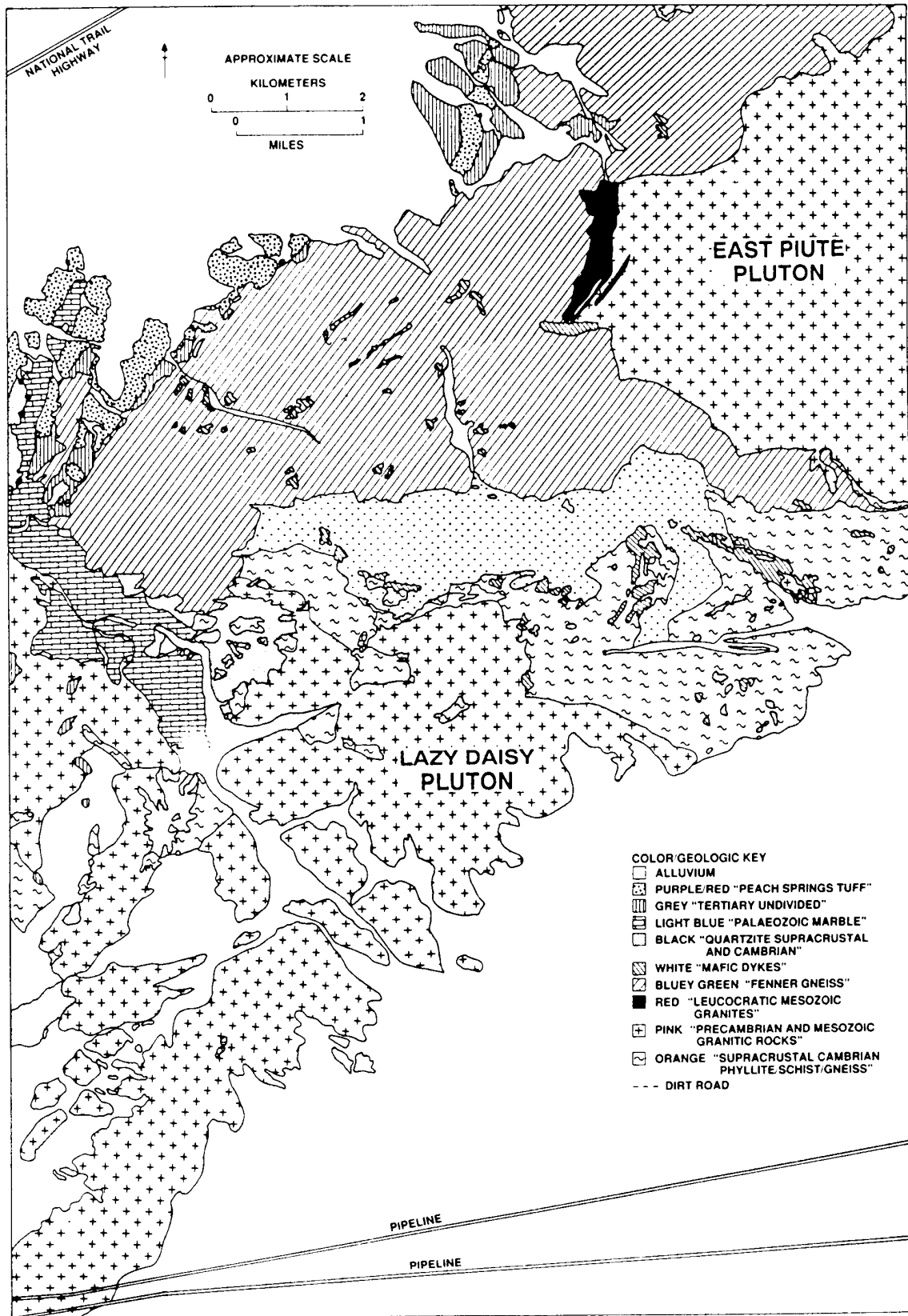
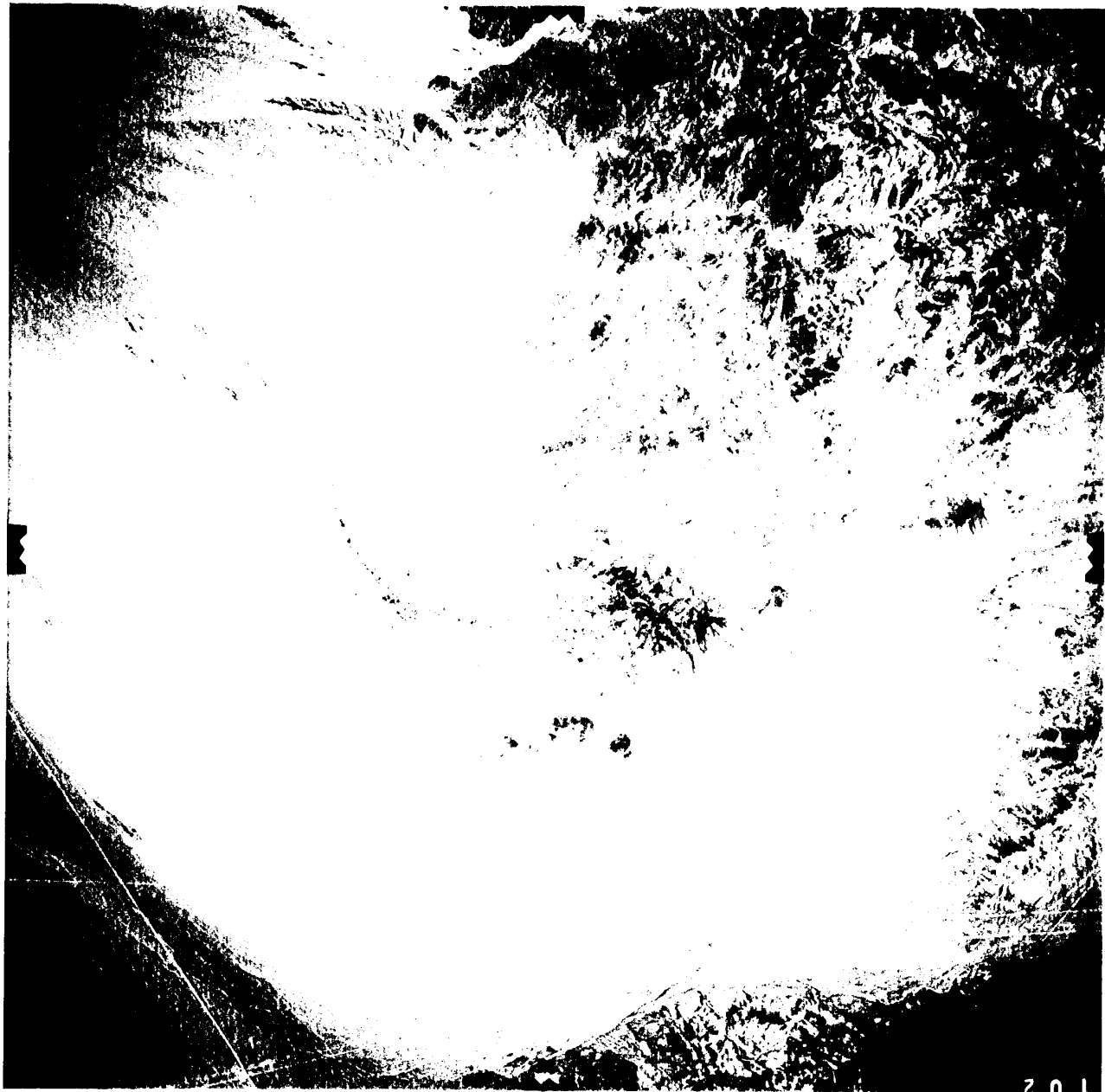


Figure 8



1944-11



201

Figure 10

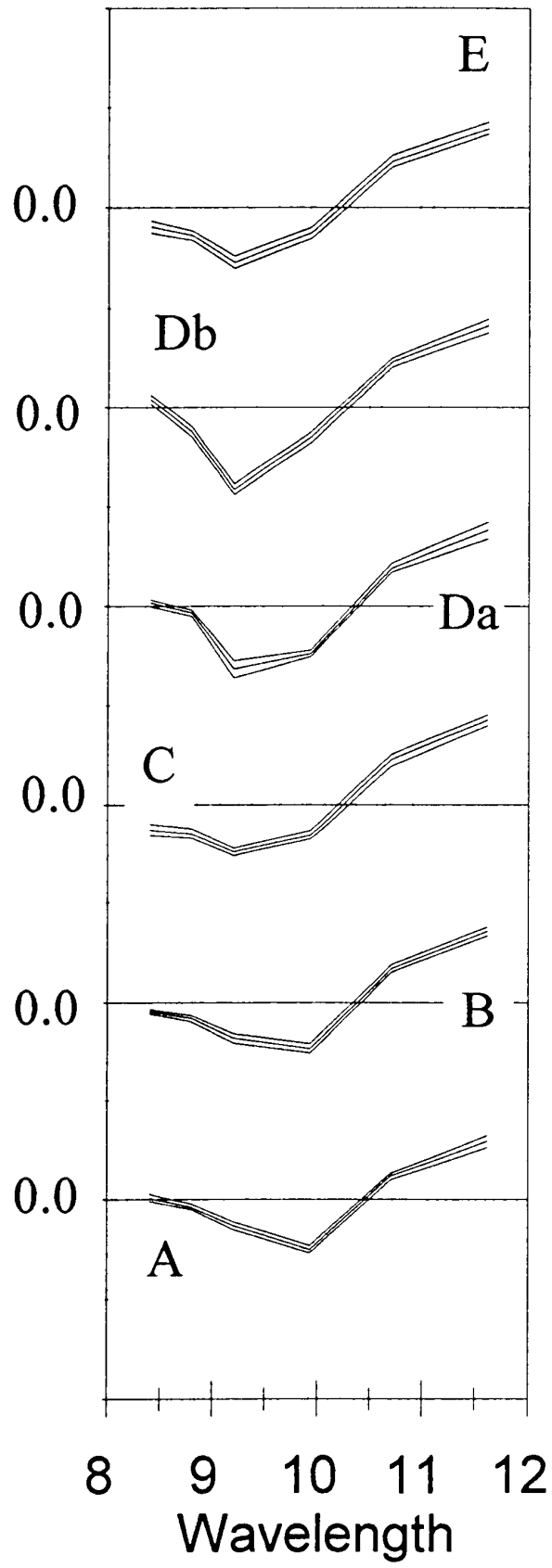
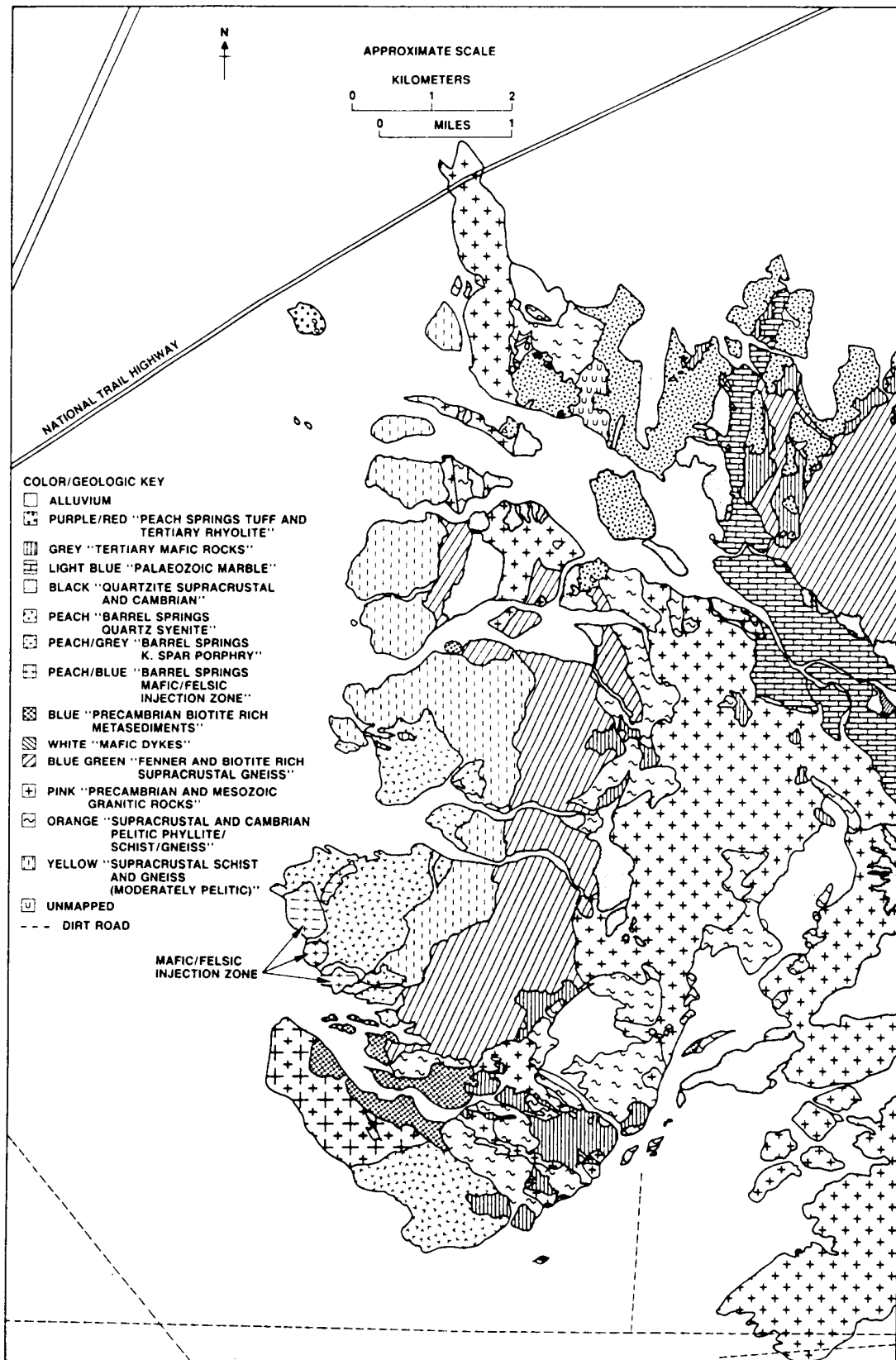


Figure 11



**SPECTRAL CONSIDERATIONS**

August 10, 1992

<b>TIMS</b>		
Wavelength Region	Band Number	Band Center
TIR	1	8.383
	2	8.785
	3	9.180
	4	9.892
	5	10.733
	6	11.655

**OTHER CONSIDERATIONS**

<b>TIMS</b>	
Instantaneous Field of View	2.5 milliradians
Total Field of View	76.56

Table 1

**SPECTRAL CONSIDERATIONS**

August 10, 1992

ASTER		
Wavelength Region	Band Number	Spectral Range
VNIR	1	0.52-0.60
	2	0.63-0.69
	3	0.76-0.86 *
SWIR	4	1.60-1.70
	5	2.145-2.185
	6	2.185-2.225
	7	2.235-2.285
	8	2.295-2.365
	9	2.360-2.430
TIR	10	8.125-8.475
	11	8.475-8.825
	12	8.925-9.275
	13	10.25-10.95
	14	10.95-11.65

**SPATIAL CONSIDERATIONS**

ASTER	
VNIR	15m
SWIR	30m
TIR	90m

**OTHER CONSIDERATIONS**

ASTER	
*STEREO BAND	YES (15m)
SWATH WIDTH	60km
POINTING	
VNIR	+/- 24 deg
SWIR	+/- 8.55 deg
TIR	+/- 8.55 deg

Table 2